AGU ADVANCING EARTH AND SPACE SCIENCES

Geophysical Research Letters

RESEARCH LETTER
10.1029/2025GL116872

Representation of Surface Mixed-Layer Eddies Affects the Large-Scale Ventilation of the Global Ocean

Takaya Uchida (内田貴也)[1,2,3], Abigail Bodner[4,5], Brandon G. Reichl[6], Alistair J. Adcroft[7], Baylor Fox-Kemper[8], Mehmet Ilicak[9,10], Mats Bentsen[10], Gustavo M. Marques[11], and William G. Large[11]

[1]Center for Ocean-Atmospheric Prediction Studies (COAPS), Florida State University, Tallahassee, FL, USA, [2]Université Grenoble Alpes, CNRS, INRAE, IRD, Grenoble INP, Institut des Géosciences de L'Environnement, Grenoble, France, [3]Now at Climate Dynamics Laboratory, Center for Earth Sciences, Moscow Institute of Physics and Technology, Dolgoprudny, Russia, [4]Department of Earth, Atmospheric, and Planetary Sciences (EAPS), Massachusetts Institute of Technology, Cambridge, MA, USA, [5]Department of Electrical Engineering and Computer Science (EECS), Massachusetts Institute of Technology, Cambridge, MA, USA, [6]Geophysical Fluid Dynamics Laboratory (GFDL), National Oceanic and Atmospheric Administration, Princeton, NJ, USA, [7]Atmospheric and Oceanic Sciences Program, Princeton University, Princeton, NJ, USA, [8]Department of Earth, Environmental, and Planetary Sciences, Brown University, Providence, RI, USA, [9]Eurasia Institute of Earth Sciences, Istanbul Technical University, Istanbul, Turkiye, [10]NORCE Norwegian Research Centre, Bjerknes Centre for Climate Research, Bergen, Norway, [11]Climate and Global Dynamics Laboratory, National Center for Atmospheric Research, Boulder, CO, USA

Key Points:

- We compare two mixed-layer eddy (MLE) parametrizations: Fox-Kemper et al. (2011, https://doi.org/10.1016/j.ocemod.2010.09.002 BFF11) and Bodner et al. (2023, https://doi.org/10.1175/jpo-d-21-0297.1 BOD23)
- BOD23 predicts finer spatial features and larger amplitudes in the submesoscale vertical buoyancy flux (SVBF)
- Ventilation of the abyssal ocean and Atlantic Meridional Overturning Circulation are sensitive to the choice of MLE parametrization in three global ocean models

Supporting Information:

Supporting Information may be found in the online version of this article.

Correspondence to:

A. Bodner,
abodner@mit.edu

Citation:

Uchida, T., Bodner, A., Reichl, B. G., Adcroft, A. J., Fox-Kemper, B., Ilicak, M., et al. (2026). Representation of surface mixed-layer eddies affects the large-scale ventilation of the global ocean. *Geophysical Research Letters*, *53*, e2025GL116872. https://doi.org/10.1029/2025GL116872

Received 20 MAY 2025
Accepted 18 DEC 2025

Author Contributions:

Conceptualization: Takaya Uchida, Abigail Bodner, Baylor Fox-Kemper
Data curation: Takaya Uchida, Abigail Bodner, Brandon G. Reichl, Alistair J. Adcroft, Mehmet Ilicak, Mats Bentsen, Gustavo M. Marques, William G. Large
Formal analysis: Takaya Uchida, Abigail Bodner

Abstract Surface mixed-layer dynamics play a crucial role in modulating the climate as it is the oceanic layer that directly communicates with the atmosphere. The resolution of global ocean models is, however, often restricted to $\mathcal{O}(1/4°)$; this is too coarse to adequately resolve mixed-layer processes, and we depend on parametrizations. One of such parametrizations is the mixed-layer eddy (MLE) parametrization. Here, we compare the performance of two MLE parametrizations [Fox-Kemper et al. (2011, https://doi.org/10.1016/j.ocemod.2010.09.002 hereon BFF11) and Bodner et al. (2023, https://doi.org/10.1175/jpo-d-21-0297.1 hereon BOD23)], and document their impact in three global ocean simulations. Upon tuning, and diagnosing submesoscale-permitting truth simulations, the MLE efficiency coefficient in BOD23 ranges between the values of 0.003–0.038, while 0.06 to 0.07 for BFF11. We find that the spatial distribution of mixed-layer depth and ventilation of the abyssal ocean, using the ideal-age tracer and Atlantic Meridional Overturning Circulation as its proxy, are sensitive to the interaction between MLE parametrizations and ocean surface boundary-layer mixing schemes.

Plain Language Summary For robust projections of the future climate, we depend on well designed numerical models of the climate. In an ideal world, the best numerical model would be where we explicitly resolve the full spectrum of scales from a few millimeters to thousands of kilometers and milliseconds to a millenia. Due to finite computational, financial and human resources, the finest spatial resolution we can push the ocean component of climate models to is currently on the order of tens of kilometers and hundreds of seconds. Namely, our models incompletely represent the phenomena below this spatiotemporal scale. As such, we need to implicitly and approximately express these unresolved phenomena and their feedback onto the resolved phenomena via methods of parametrizations. Here, we document the impact of two parametrizations, which mimic the behavior of oceanic surface currents on the scales of a few kilometers, on the global ocean.

1. Introduction

While the day may arrive sooner than was once imagined where we resolve the climate system down to the Kolmogorov scale (Fox-Kemper et al., 2014), with the aid of Graphic Processing Units (GPUs; Häfner et al., 2021; Silvestri et al., 2023; Wei et al., 2024), we are still far from having the adequate resources to do so (Hewitt et al., 2022). The storing, distributing and post-processing of peta-bytes of model outputs also presents itself as a formidable bottleneck to the scientific community in effectively utilizing the data (Abdulah et al., 2024; Bai et al., 2023; Govett et al., 2024; Panta et al., 2024; Uchida et al., 2022; Zhang et al., 2023). Furthermore, resolving the oceans and climate down to the molecular scale will inevitably present itself with the same daunting level of complexity as of the real natural world. For practical reasons, the spatial resolution of global ocean models used in Coupled Model Intercomparison Project (CMIP) simulations has remained on the order of

Investigation: Takaya Uchida, Abigail Bodner, Brandon G. Reichl, Alistair J. Adcroft, Baylor Fox-Kemper, Mehmet Ilicak, Mats Bentsen, Gustavo M. Marques, William G. Large
Methodology: Takaya Uchida, Abigail Bodner, Baylor Fox-Kemper
Project administration: Takaya Uchida, Abigail Bodner
Resources: Takaya Uchida, Abigail Bodner, Brandon G. Reichl, Alistair J. Adcroft, Mehmet Ilicak, Mats Bentsen, Gustavo M. Marques, William G. Large
Software: Takaya Uchida, Abigail Bodner, Brandon G. Reichl, Alistair J. Adcroft, Mehmet Ilicak, Mats Bentsen, Gustavo M. Marques, William G. Large
Supervision: Takaya Uchida, Abigail Bodner, Alistair J. Adcroft, Baylor Fox-Kemper
Validation: Takaya Uchida, Abigail Bodner, Brandon G. Reichl, Alistair J. Adcroft, Baylor Fox-Kemper, Mehmet Ilicak, Mats Bentsen, Gustavo M. Marques, William G. Large
Visualization: Takaya Uchida, Abigail Bodner, Brandon G. Reichl, Mehmet Ilicak, Mats Bentsen, Gustavo M. Marques, William G. Large
Writing – original draft: Takaya Uchida, Abigail Bodner
Writing – review & editing: Takaya Uchida, Abigail Bodner, Brandon G. Reichl, Baylor Fox-Kemper, Mehmet Ilicak, Mats Bentsen, Gustavo M. Marques

1°–1/16° (Chassignet et al., 2020; Eyring et al., 2016; Moon et al., 2025; Silvestri et al., 2025; Treguier et al., 2023; Uchida et al., 2017). As such, we will continue to rely on eddy parametrizations, which implicitly represent the sub-grid effects onto the resolved flow. Parametrizations, in a way, lie at the frontier of our understanding of natural phenomena and it should be emphasized that the development of parametrizations enhances our physical interpretation of the system in addition to improving numerical models.

Here, we focus on a particular parametrization that represents the effects of submesoscale $\mathcal{O}$(1–10 km) eddies within the oceanic mixed layer, often referred to as the mixed-layer eddy (MLE) parametrization (Boccaletti et al., 2007; Fox-Kemper et al., 2011, hereon referred to as BFF11). The MLE parametrization mimics the effects of submesoscale baroclinic instability (SBI) within the mixed layer where available potential energy is released to restratify the layer. Since there is a well-developed theory of SBI (Stone, 1966), the resolution of models needed to resolve these instabilities have been argued to be $\mathcal{O}$(1 km) in global simulations (Dong et al., 2020; Uchida et al., 2019, 2020). The BFF11 parametrization has been widely adopted in CMIP simulations and has been documented to reduce the model biases in mixed-layer depth (MLD; Calvert et al., 2020; Fox-Kemper et al., 2011; Griffies et al., 2016, 2025b; Smith et al., 2025). This has significant implications on modeling the climate as the heat flux through the mixed-layer directly modulates the air-sea fluxes of heat and momentum (Bai et al., 2023; Busecke et al., 2025; Conejero et al., 2024; Jamet et al., 2024), and ventilation of deeper waters through mode waters (Deremble & Dewar, 2013; Dewar, 1986; Forget et al., 2011; Maze & Marshall, 2011; Sun et al., 2025) and deep-water formation (Tagklis et al., 2020). Furthermore, it has been argued that the ocean carbon cycle is sensitive to the representation of the mixed layer (Boyd et al., 2019; Lévy et al., 2013).

Recently, Bodner et al. (2023, hereon referred to as BOD23) proposed an amelioration to the MLE parametrization to incorporate turbulence-influenced frontogenetic tendencies. BFF11 acknowledged that the determination of frontal widths, which is generally unresolved, was a source of uncertainty in their formulation, quoting "*No compelling theory for the width of oceanic mixed layer fronts is known to the authors*." The breakthrough that BOD23 provided is a physically consistent estimate of the surface frontal width based on boundary-layer process scaling arguments. In the following text, we will document how the BFF11 and BOD23 formulations of the parametrization affect: (a) the prediction of submesoscale vertical buoyancy flux (SVBF) from kilometric-resolution simulations in the separated Gulf Stream region, and (b) MLD, oceanic ventilation, and Atlantic Meridional Overturning Circulation (AMOC) in global ocean simulations at non-eddying to eddying resolutions. This set of metrics centers around the climate impacts of submesoscales on global ocean heat and carbon uptake (Fox-Kemper et al., 2021; Griffies & Greatbatch, 2012) and oxygenation of the ocean interior (Busecke et al., 2022; Naveira Garabato et al., 2017).

2. Data and Method

2.1. Global Ocean Simulations

The Geophysical Fluid Dynamics Laboratory (GFDL) twin global 1/4° ocean simulations (with BFF11 or BOD23) were produced using the Modular Ocean Model (MOM6) in hybrid geopotential-sigma2 coordinates; they were both spun up from a state of rest using OM4p25 (Adcroft et al., 2019, https://github.com/NOAA-GFDL/MOM6.git). The initial conditions for potential temperature and practical salinity were taken from the World Ocean Atlas 2013 (WOA13; Levitus et al., 2014) database. The OM4p25 simulations contain a few updates to OM4 relative to (Adcroft et al., 2019). The ocean surface boundary-layer (OSBL) mixing uses the energetics-based Planetary Boundary Layer (ePBL; Reichl & Hallberg, 2018) that was updated to improve fidelity of mixing in near-equatorial (±5°) latitudes (Reichl et al., 2024). The bottom boundary-layer efficiency was reduced from 0.2 to 0.01, which improves biases related to excessive bottom boundary-layer mixing in coastal regions (Griffies et al., 2025a). A new horizontal discretization of the Jackson et al. (2008) shear-driven mixing is adopted that suppresses grid-scale numerical noise (Griffies et al., 2025a). Given that BOD23 is a newer parametrization, the run with BOD23 was tuned (MLE efficiency coefficient, $C_r = 0.038$) so as to have similar global heat uptake to the BFF11 run ($C_e = 0.07$; blue curves in Figure 1a). The simulation was spun up for one iteration of 1958–2022 and we will be using the second iteration of 1958–2022 as outputs.

The Community Earth System Model (CESM) twin global ocean simulations also adopt MOM6 but with different settings from GFDL (Marques et al., 2023, https://github.com/ESCOMP/MOM_interface/wiki/Detailed-Instructions). CESM MOM6 employs a modified K-profile parametrization (KPP; Large et al., 1994), which accounts for: (a) a non-local momentum flux in the wind direction when it is not aligned with local shear, and

10.1029/2025GL116872

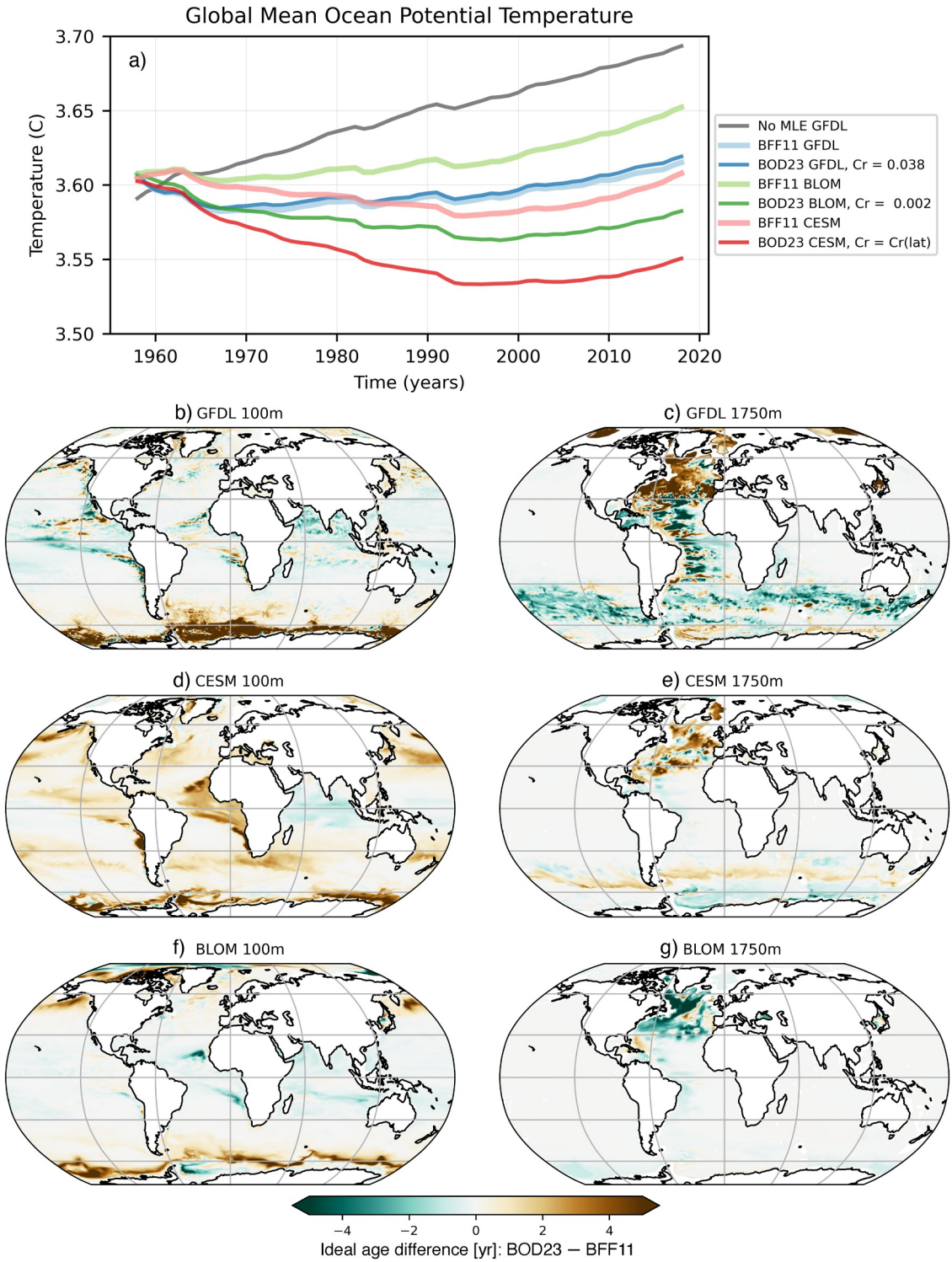

Figure 1. Time series of the global volume-averaged potential temperature [°C] from the runs with BFF11 and BOD23 from the 0.25° Geophysical Fluid Dynamics Laboratory (GFDL) with ePBL (blue curves), 2/3° Community Earth System Model (CESM) with modified KPP (red curves), and 1° BLOM with CVMix KPP (green curves) between 1958 and 2018 (a). The GFDL run without mixed-layer eddy (MLE) parametrizations is shown in gray curves. The light solid curves document the BFF11 runs and dark solid curves the BOD23 runs. C_r in the BOD23 CESM implementation varies in latitude. Reducing the values of C_r to 0.03 in GFDL led to more heat uptake and a warmer ocean (not shown). Differences in ideal age between the twin runs given by the two versions of the MLE parameterization at 100 m (left column) and 1750 m (right column) depths (b–g). Positive values indicate that BOD23 leads to weaker ventilation of the water column and vice versa. Outputs from the last 5 years of each cycle are averaged.

(b) mixing induced by waves following the expanded Monin-Obukhov Similarity Theory to include Stokes drift (Large et al., 2021). The model resolution is nominal 2/3° but is enhanced merdionally to 1/4° around the Equator. The latitude-dependent diapycnal diffusivity due to internal wave mixing defined in Danabasoglu et al. (2012) is included. Energy dissipation from tidally induced diapycnal mixing is represented using Simmons et al. (2004). The simulations start from a state of rest with the initial potential temperature and salinity fields taken from the January climatology of the World Ocean Atlas 2018 (WOA18; Boyer et al., 2018). BOD23 was tuned (latitudinally varying C_r) to have similar strengths in the MLE streamfunction as BFF11 in the Southern Ocean ($C_e = 0.07$). The simulation was run for one iteration during 1958–2018.

The Bergen Layered Ocean Model (BLOM; https://github.com/NorESMhub/BLOM) is a state-of-the-art hydrostatic and non-Boussinesq ocean model, horizontally discretized on the Arakawa-C grid. BLOM is the ocean component of the Norwegian Earth System Model and uses 56 vertical levels with a tripolar horizontal grid. The model resolution is nominal 1°; about the Equator, it is enhanced to 1/4° meridionally. A notable update compared to the CMIP6 version (Seland et al., 2020) is the Arbitrary Lagrangian Eulerian (ALE) method, permitting a hybrid vertical coordinate. With enhanced vertical resolution compared to the previous bulk mixed-layer formulation, a submesoscale eddy-driven overturning can now be represented. For OSBL physics and shear-driven vertical mixing, BLOM with ALE employs KPP as implemented in the CVMix package (Griffies et al., 2015). Compared to Large et al. (1994), a parabolic shape function is used for non-local surface fluxes of freshwater, non-solar heat and momentum, while non-local flux due to brine release uses a shape function that leads to brine absorption near the base of the mixed layer. Tidally driven diapycnal mixing follows the parameterization by Simmons et al. (2004) where the conversion of tidal energy to internal waves is estimated by Jayne (2009). The BLOM simulations were initialized from a state of rest using temperature and salinity fields from the Polar science center Hydrographic Climatology (PHC) 3.0 (updated from Steele et al., 2001). They were integrated over a 61-year period, 1958–2018. BOD23 was tuned ($C_r = 0.003$) so as to have similar strengths in the MLE stream function as BFF11 ($C_e = 0.06$).

All of the simulations were atmospherically forced using the Japanese Reanalysis product (JRA55-do; Tsujino et al., 2018), and they include a surface salinity restoring with a piston velocity of 0.1667 m day^{-1}, corresponding to ∼300 days over 50 m, following Danabasoglu et al. (2014). Mesoscale eddies in CESM MOM6 and BLOM are parameterized via the Gent-McWilliams' skew diffusion (GM; Gent & McWilliams, 1990; Griffies, 2018) in conjunction with tracer diffusion along neutral directions (Redi, 1982). BLOM employs the scheme of Shao et al. (2020) and eddy diffusivity is estimated with a bottom-slope aware parameterization (Nummelin & Isachsen, 2024). We will use the last 20 years of output from each simulation. Figure 1a demonstrates the time evolution of global volume-averaged potential temperature in all of the runs. Except for GFDL where the target of tuning for BFF11 and BOD23 was global heat uptake, BOD23 generally results in a colder ocean.

2.2. Submesoscale-Permitting North Atlantic Simulations

We use daily-averaged outputs during boreal early spring (February - April) from a 1/60° North Atlantic simulation in geopotential coordinates based on the Nucleus for European Modeling of the Ocean model (eNATL60; Brodeau et al., 2020) and 1/50° North Atlantic simulation in hybrid coordinates based on the HYbrid Coordinate Ocean Model (HYCOM50; Xu et al., 2022). Both simulations are atmospherically and tidally forced, and have one of the highest resolutions to date for simulations that cover the North Atlantic basin, 26°N to 65°N and 28°S to 80°N respectively. An assessment on the realism of eNATL60 and HYCOM50 appears in Chassignet and Xu (2017), Ajayi et al. (2020, 2021) and Xu et al. (2022). Our choice of using eNATL60 and HYCOM50 outputs is motivated by the fact that the ALE algorithm of MOM6 and BLOM allows for geopotential, isopycnal or hybrid coordinate systems (Marques et al., 2023).

2.3. Formulation of the MLE Parametrization

The MLE parametrization predicts that the bulk of SVBF, $\overline{w^s b^{s^z}}$, can be approximated by the lateral gradients of the mesoscale buoyancy field, $\nabla_h b^m$,

$$\langle \overline{w^s b^{s^z}} \rangle \simeq C\Psi \times \overline{\nabla_h \langle b^m \rangle^z}, \tag{1}$$

where $\langle\cdot\rangle$ is a horizontally coarse-graining operator, ∇_h is taken over the mixed layer and $\overline{(\cdot)}^z$ is a vertical averaging over the MLD. The spatial coarsening is taken after the vertical averaging for SVBF to account for the fact that climate models generally have vertical resolutions too coarse to resolve the submesoscales; the two operations do not exactly commute due to the local dependency on MLD. The mesoscale buoyancy fields, b^m, were horizontally coarsened prior to taking the horizontal gradients to mimic the resolved buoyancy fields in climate simulations.

Two formulations for the MLE stream function $\boldsymbol{\Psi}$ have been proposed and implemented in the GFDL MOM6, CESM MOM6 and BLOM code (Boccaletti et al., 2007; Fox-Kemper et al., 2008, 2011, hereon BFF11):

$$\boldsymbol{\Psi}^{\mathrm{BFF11}} \overset{\mathrm{def}}{=} \frac{\Delta s}{\langle L_{\mathrm{ML}}\rangle} \frac{\langle H\rangle^2 \overline{\nabla_h \langle b^m\rangle}^z \times \mathbf{z}}{\langle |f|\rangle}, \tag{2}$$

and (Bodner et al., 2023, hereon BOD23):

$$\boldsymbol{\Psi}^{\mathrm{BOD23}} \overset{\mathrm{def}}{=} \frac{\Delta s}{\langle L_f/C_L\rangle} \frac{\langle H\rangle^2 \overline{\nabla_h \langle b^m\rangle}^z \times \mathbf{z}}{\langle |f|\rangle}, \tag{3}$$

where $\mathbf{z}$ is the vertical unit vector. The tuning parameter (or efficiency coefficient) for BFF11 is $C = C_e(t)$ and for BOD23 $C = C_r(t)$ in (1). $L_{\mathrm{ML}} = \frac{NH}{|f|}$ is the mixed-layer Rossby radii where H and $N = \sqrt{\overline{N^2}^z}$ are the MLD and buoyancy frequency respectively and f is the local Coriolis frequency. Although N^2 may be small and ill defined within parts of the mixed layer, the definition of MLD as the depth where potential density increases by a certain threshold naturally implies that $N^2\left(\propto -\frac{\partial\rho}{\partial z}\right)$ is never always arbitrarily small over the entire mixed layer. $L_f = C_L \frac{\left(m_* u_*^3 + n_* w_*^3\right)^{2/3}}{f^2 h}$ is the frontal width set by turbulent thermal-wind balance where h is the boundary-layer depth (BLD), $u_* = \sqrt{\tau^{x2} + \tau^{y2}}/\rho_0$ and $w_* = (B_0/h)^{1/3}$ are the turbulent-friction and convective velocities respectively, and $m_*, n_* = 0.5, 0.066$. Note that the mixed layer is defined by a layer with relatively uniform stratification while the boundary layer is where active surface-forced mixing is taking place; the former is generally deeper than the latter ($|H| \gtrsim |h|$) during convective conditions (Sutherland et al., 2014). GFDL MOM6 takes h from ePBL and H by temporally filtering h. In CESM MOM6, BLD diagnosed by KPP is used as h, while H is defined as the depth where σ_0 increases by 0.02 kg m^{-3} relative to the surface. To account for the diurnal cycle, H is time-filtered following the method described in Adcroft et al. (2019). BLOM also takes h from KPP but determines H using the σ_0 criteria of 0.03 kg m^{-3}.

For the offline diagnostics of eNATL60 and HYCOM50, we have approximated BLD as $h \approx 0.7 h_{\mathrm{Ek}}$ where $h_{\mathrm{Ek}} = u_*/f$ is the Ekman depth, since BLD was not saved as model outputs. The 0.7 factor is there to account for the fact that BLD tends to be shallower than the Ekman depth (Reichl & Hallberg, 2018, their Figure 5). In theory, approximating BLD by the Ekman depth would reduce to zero under pure convection but the wind-stress magnitude was never zero in the domain we analyzed (not shown). $B_0 = g\alpha \frac{Q}{\rho_a c_p}$ is the surface buoyancy flux and Q [W m^{-2}] is the outgoing surface heat flux from the ocean, that is, $Q > 0$ when the ocean is warming the atmosphere. α is the thermal expansion coefficient of seawater. The ocean and atmospheric reference densities were set to $\rho_0 = 1000$ kg m^{-3} and $\rho_a = 1.225$ kg m^{-3}, and $c_p = 1005$ J kg^{-1} K^{-1}. Further details on the variables are left to BFF11 and BOD23.

We take an approach similar to Uchida et al. (2022) where we intercompare two submesoscale-permitting realistic ocean simulations, eNATL60 and HYCOM50, in the separated Gulf Stream region. Buoyancy was defined using potential density in reference to 0 dbar, $b = -g\frac{\sigma_0}{\rho_0}$. MLD was defined using the density criterion (de Boyer Montégut et al., 2004), viz., the depth at which $\sigma_0 = \rho - \rho_0$ increased by 0.03 kg m^{-3} from its value at ∼10 m depth (Treguier et al., 2023). The meso- and submeso-scale fields were decomposed using a Gaussian filter with the standard deviation of 30 km (Grooms et al., 2021), for example, $b = b^m + b^s$. We chose the coarse-graining operator as 15 × 15 and 12 × 12 grid points respectively so as to coarsen the eNATL60 diagnostics to ∼1/4° and HYCOM50 to ∼0.24°; namely, the finest limit of spatial resolution where the MLE parametrization may be

turned on in climate simulations (Adcroft et al., 2019; Storkey et al., 2024). The resolution factor was set as the square root of the local coarsened grid area, $\Delta s = \sqrt{\langle \mathcal{A} \rangle}$ where $\mathcal{A}$ is the horizontal grid area of the raw model outputs. The efficiency coefficients were diagnosed by taking the ratio between the left- and right-hand sides of (1), $C(t,y,x) = \frac{\overline{\langle w^s b^s \rangle}^z}{\Psi \times \overline{\nabla_h \langle b^m \rangle}^z}$, and then estimated as their spatial median. Namely, the diagnosed coefficients vary in time but are constants in space. We will compare the diagnosed coefficients with the recommended values in BFF11 and BOD23.

3. Results

3.1. Comparison of MLE Parametrizations

Figure 2 documents the comparison between SVBF and its prediction from BFF11 and BOD23. Given that the two simulations are internal-tide permitting, SVBF here captures the net effect of eddy-eddy and eddy-wave interactions at kilometric model resolution. Submesoscale vertical buoyancy flux is generally in the direction of restratifying the mixed layer ($\overline{\langle w^s b^s \rangle}^z > 0$; Figures 2a, 2f, 2g, and 2l). The order of magnitude of the spatial median of SVBF, $\mathcal{O}(5 \times 10^{-9}\ \mathrm{m^2\ s^{-3}})$ with spatial extrema reaching up to $\mathcal{O}(10^{-7}\ \mathrm{m^2\ s^{-3}})$, tends to fall within the range of observational estimates (Buckingham et al., 2019; Johnson et al., 2016, 2020; Mahadevan et al., 2012). Both parametrizations capture the mesoscale fronts associated with the separated Gulf Stream but the cumulative isotropic wavenumber cross spectra of BOD23 is higher than BFF11 at scales larger than 100 km (Figures 2c and 2i), the effective resolution of CMIP-class ocean simulations (Masson-Delmotte et al., 2021). Namely, BOD23 leads to more restratification than BFF11 about the Gulf Stream.

The time series of BFF11 and BOD23 demonstrate that both are able to track SVBF (Figures 2f and 2l) with the caveat that the C is a tuning parameter. The efficiency coefficients are farther for BOD23 than BFF11 to their respective recommended values $C_r (= C_e / C_L) = 0.24$–0.32 (Bodner et al., 2023) and $C_e = 0.06$ 0.08 (Fox-Kemper et al., 2011) during times of vigorous restratification (Figures 2e and 2k). Another scaling for C_r can be argued for by assuming that the recommended values above for C_e are for cases where the frontal width is approximated by the mixed-layer Rossby radii.

$$C_e \Psi^{\mathrm{BFF11}} \times \overline{\nabla_h \langle b^m \rangle}^z \sim C_r \Psi^{\mathrm{BOD23}} \times \overline{\nabla_h \langle b^m \rangle}^z, \tag{4a}$$

$$\therefore\ C_r \sim \frac{L_f / C_L}{L_{\mathrm{ML}}} C_e, \tag{4b}$$

Which differs from Bodner et al. (2023, their Equation 27). Given the characteristic values of $C_L \sim 0.25$, $L_{\mathrm{ML}} \sim 1$ km and $L_f \sim 100$ m, (4b) yields $C_r \sim 2.4 \times 10^{-3}$–$3.2 \times 10^{-3}$. These values align more closely to C_r diagnosed from eNATL60 and HYCOM50 (Figure 2). Alternatively, were L_{ML} in (2) replaced by L_f, the values of C_e should be smaller. When the efficient coefficients are set as constants, viz. Their time mean ($\overline{C_r}^t = (6.5, 3.4) \times 10^{-4}$, $\overline{C_e}^t = (8.6, 6.0) \times 10^{-3}$ for eNATL60 and HYCOM50 respectively), the performance slightly deteriorates but the parametrizations are still able to predict the enhanced restratification that takes place during February and lower levels from March onwards (dashed curves in Figures 2f and 2l). Based on scaling arguments, the MLE stream function is proportional to the BLD by $\Psi^{\mathrm{BOD23}} \propto h^{5/3}$. It is possible that the Ekman depth, taken for diagnostic purposes, underestimates the BLD in certain scenarios but this means that using the true BLD would lead to even smaller "C_r"s; this works in favor of our recommendation of using smaller C_r values than recommended by Bodner et al. (2023).

3.2. Ventilation of the Global Ocean

Figure 3 documents the 5-year averaged MLD from the GFDL, CESM and BLOM runs. Mixed-layer depth here was defined using potential-density metrics, that is, the depth at which σ_0 exceeded its value at $\sim$10 m depth by 0.03 kg m^{-3} (de Boyer Montégut et al., 2004), to be consistent with observational estimates from the ARGO floats. This diagnostic approach differs slightly from MLD used in the online calculations of H in (1–3) (cf., Section 2.3). It is common, however, to uniformly employ the same potential-density metric for model assessment (Treguier et al., 2023). In the zonal-mean sense, GFDL has the deepest MLDs, which come closest to the ARGO estimates, and BLOM has the shallowest MLDs (Figures 3a and 3b). However, all of the

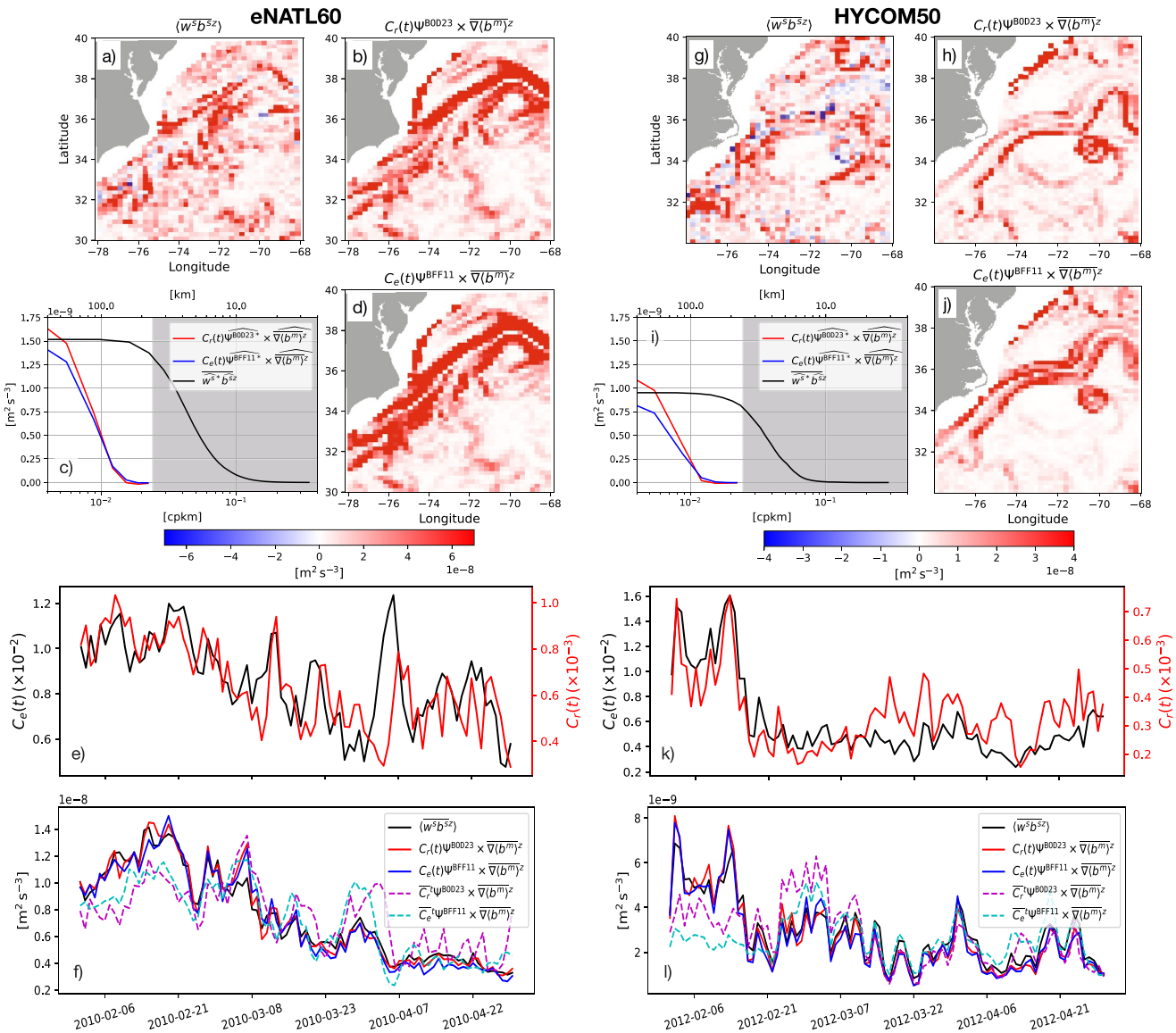

Figure 2. Submesoscale vertical buoyancy flux (SVBF; $\langle \overline{w^s b^{sz}} \rangle$) and its prediction by BOD23 and BFF11 where bathymetry is deeper than 200 m. Spatial maps of them on Feb. 1 from eNATL60 (a, b, and d) and HYCOM50 (g, h, and j). Cumulative isotropic wavenumber cross spectra of SVBF over 30°–37°N, 68°–74°W; black solid) and predictions from BOD23 (red solid) and BFF11 (blue solid) for the three months of February–April. (c, i). The gray shading indicates the wavenumber cutoff due to the coarse graining, $\langle \mathcal{A} \rangle^{-1/2}$. The cumulative cross spectra were constructed as $\int_{k' > k} \Re\left[\widehat{w^s}^* \widehat{b^s}\right] dk'$ averaged over the top 100 m for SVBF and $\int_{k' > k} \Re\left[C\hat{\mathbf{\Psi}}^* \times \widehat{\nabla_h \langle b^m \rangle^z}\right] dk'$ for the parametrizations. The Fourier transforms $\widehat{(\cdot)}$ were taken every 14 days with the Hann window applied, * is the complex conjugate and $\Re[\cdot]$ is the real part. Note that the SVBF cross spectra were not coarse grained as we are interested in the submesoscale covariance, cf., $\widehat{\langle w^s \rangle}^* \widehat{\langle b^s \rangle} \neq |\widehat{\langle w^s b^s \rangle}|$. Time series of the spatial median of $C_e(t, y, x)$ (black solid plotted against the left y axis) and $C_r(t, y, x)$ (red solid plotted against the right y axis) (e, k). Time series of the spatial median of SVBF and its predictions from BOD23 and BFF11 (f, l). The dashed curves are when time-averaged values of the efficiency coefficients are used.

simulations fail to reproduce the deep MLDs north of 50°N during winter. A similar shallow bias is seen across the global equatorial region during summer. As a point of reference, we also document the GFDL run when no MLE parametrizations are turned on (gray curves in Figures 3a and 3b). Interestingly, the GFDL no-MLE run comes closer to observations in the zonal-mean sense than the MLE runs outside of the Southern Ocean but MLD in the Southern Ocean ends up too deep. The difference between BOD23 and BFF11 appear to be minor when zonally averaged but their heterogenous spatial patterns become apparent when global maps are examined.

10.1029/2025GL116872

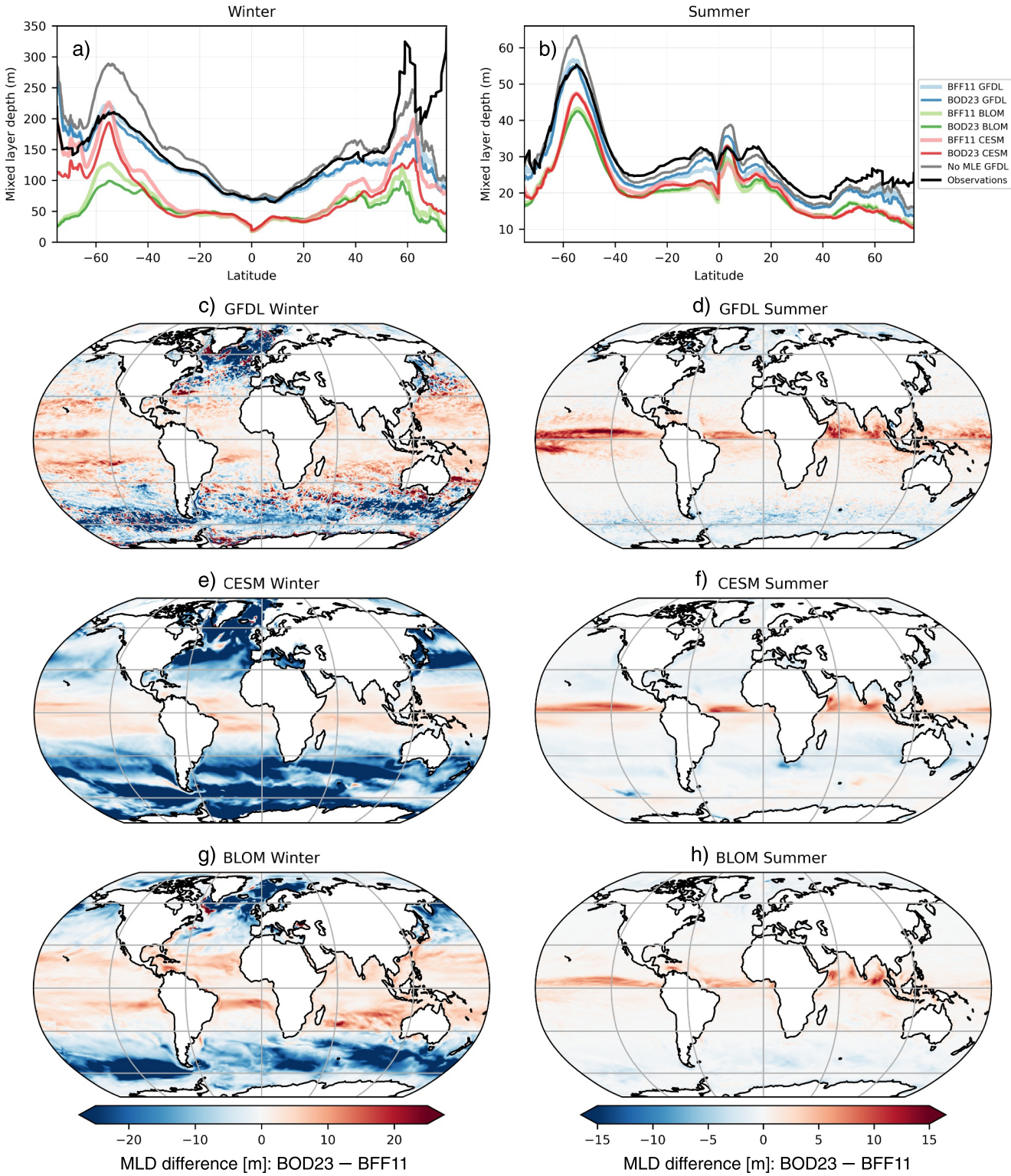

Figure 3. Mixed-layer depth estimates from ARGO and the BOD23 and BFF11 runs for global boreal and austral winter (left column), and boreal and austral summer (right column). Zonal-mean MLDs are given in panels (a, b). ARGO estimate is in the black curve, Geophysical Fluid Dynamics Laboratory (GFDL) runs in blue curves, Community Earth System Model runs in red curves and BLOM runs in green curves. The GFDL run without mixed-layer eddy parametrizations is shown in gray curves. Global maps of difference between the twin BOD23 and BFF11 runs are shown in panels (c–h). Negative values indicate a stronger restratification and shallower MLDs in BOD23.

First thing to note is that MLDs from the CESM and BLOM runs are much smoother in space than the GFDL run due to their coarser spatial resolution and mesoscale eddies being parametrized (Figures 3c–3h). In the tropics, a region where the mixed-layer Rossby radii L_{ML} become ill defined, BFF11 predicts shallower MLDs (i.e., more restratification) whereas in the subpolar regions BOD23 predicts shallower MLDs most notably in the North Atlantic. If one zooms into the wintertime Gulf Stream and Kuroshio regions, BOD23 also tends to predict shallower MLDs than BFF11 (Figures 3c, 3e, and 3g). In the Southern Ocean, all of the models agree that BOD23 leads to increased restratification and shallower MLDs than BFF11 particularly in wintertime.

As a proxy for ocean ventilation, we show the ideal age tracer, which has been included as part of the CMIP protocol since CMIP6 (Orr et al., 2017), in Figures 1b–1g. Water masses recently in contact with the atmosphere have a younger age and vice versa. Within the surface mixed layer (Figures 1b, 1d, and 1f), we find that the Southern Ocean has older water masses when BOD23 is turned on compared to BFF11 consistently across all models. This is consistent with Figures 2c and 2i where BOD23 leads to more restratification of the mixed layer and, thus, less ventilation within the surface layer. Beyond this point, however, the models tend to disagree with each other; GFDL and CESM predict that BOD23 leads to less ventilation in the abyssal North Atlantic (Figures 1c and 1e) whereas BLOM indicates that BOD23 leads to more ventilation (Figure 1g). At the northern flank of the Antarctic Circumpolar Current (ACC; ∼45°S), BOD23 in GFDL has a younger age while in CESM, it is the opposite and BLOM demonstrates no significant difference. Around the tropics and subtropics, BOD23 in CESM results in less ventilation within the mixed layer (Figure 1c) but BOD23 in GFDL and BLOM results in more ventilation (Figures 1b and 1f).

We end this section by documenting the AMOC stream function north of 35°S. The AMOC stream function was defined as

$$\Psi_{\mathrm{AMOC}}(\lambda, z) = \int_{\vartheta_{\mathrm{w}}}^{\vartheta_{\mathrm{e}}} \int_{z_b}^{z} v(\lambda, \vartheta, z) \cos(\lambda) a \, \mathrm{d}z \, \mathrm{d}\vartheta, \tag{5}$$

where λ is latitude, z is depth, z_b is sea-floor depth, v is meridional velocity, a is the earth radius, ϑ is longitude spanning the zonal extent of North Atlantic (ϑ_{w} to ϑ_{e}). We find that BOD23 leads to a weakening of AMOC in GFDL and CESM but a strengthening in BLOM, all on the order of 5%–20%. Given that the deceleration of AMOC over the 20$^{\mathrm{th}}$-to-21$^{\mathrm{st}}$ century is argued to be on the order of 15% (Caesar et al., 2018), we find this sensitivity to be quite significant. The weaker AMOC is consistent with the ventilation patterns (Figures 1b and 1d), that is, older water masses below the thermocline in the North Atlantic in the BOD23-GFDL and BOD23-CESM runs. The stronger AMOC in BOD23-BLOM than BFF11-BLOM is consistent with a more coherent ventilation in the subpolar North Atlantic (Figure 1g).

4. Conclusions and Discussion

We have documented results on MLD and ventilation of the global ocean when two different MLE parametrizations, Fox-Kemper et al. (2011, BFF11) and Bodner et al. (2023, BOD23), were implemented in the GFDL MOM6, CESM MOM6 and BLOM code. BOD23 and BFF11 systematically shoal the mixed layer in GFDL MOM6 by 9% during summer and 18% over winter compared to their no-MLE counterpart (Figures 1a, 3a, and 3b and Figure S1 in Supporting Information S1). Across all models, BOD23 leads to less ventilation than BFF11 within the surface Southern Ocean (south of 50°S) on the order of 10%–39% (Figures 1b, 1d, and 1f), and BFF11 results in 4%–8% shallower MLDs in the tropics and extratropics (between 20°S–20°N) than BOD23 years round (Figures 3c–3h). The agreement ends here, however; we find that different tuning strategies between the twin runs lead to diverse realizations of the global ocean. For example, despite the GFDL twin runs being tuned to have similar global oceanic heat uptake (Figure 1a), BOD23 leads to shallower MLDs in the North Atlantic during wintertime (Figure 3c). This heightened restratification is consistent with what we find from submesoscale-permitting simulation outputs in the separated Gulf Stream region (Figure 2). Below the thermocline, BOD23-GFDL results in increased ventilation in the tropical and subtropical Atlantic compared to the other models (30°S–30°N; Figure 1c). In the abyssal subpolar North Atlantic, GFDL and CESM agree on less ventilation under BOD23 (Figures 1c and 1e) but BLOM predicts an increase in ventilation (Figure 1g). Regarding AMOC, BOD23-GFDL and BOD23-CESM predict a weakening compared to their BFF11 counterparts whereas in BLOM, the relation is opposite (Figure 4). The spatiotemporal details in MLEs have been documented to

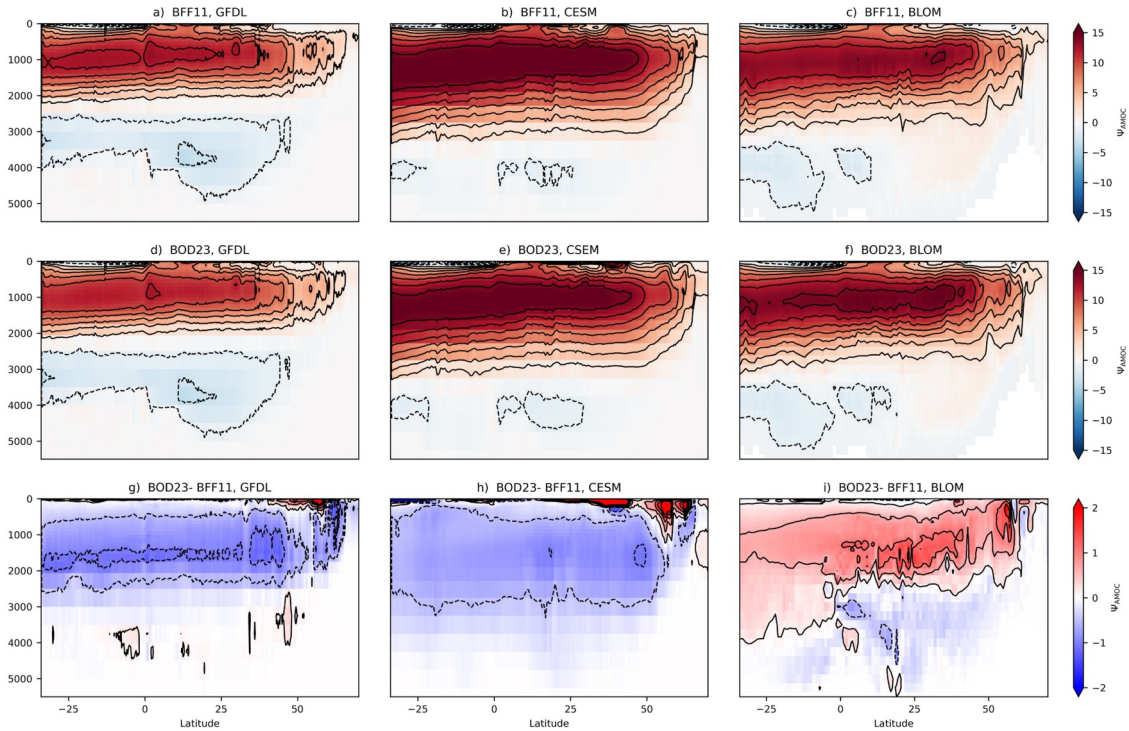

Figure 4. Atlantic Meridional Overturning Circulation (AMOC) stream function for BFF11 (top row; a–c) and BOD23 runs (middle row; d-f) averaged over the last 20 years of the outputs from Geophysical Fluid Dynamics Laboratory, Community Earth System Model and BLOM. The difference between the BOD23 and BFF11 streamfunction is shown is the bottom row where negative values indicate a spin down of AMOC in BOD23 (g–i).

modulate the formation and ventilation of subtropical mode waters (Xu et al., 2025), deep-water formation in the North Atlantic (Tagklis et al., 2020) and its subsequent contribution to AMOC (De Marez et al., 2024).

By reverse engineering the MLE parametrizations using submesoscale-permitting simulation outputs, we find that the efficiency parameter C_r is about 30% of the recommendations made by BOD23. These estimates involve two notable approximations:

1. SBI is marginally resolved in eNATL60 and HYCOM50 (Dong et al., 2020, 2021), and the turbulence that arrests frontogenesis is parameterized in these models; turbulence-front-eddy interaction with parameterized turbulence can be very different from that in large-eddy simulations (LES; Johnson & Fox-Kemper, 2024; Li et al., 2024; Sullivan & McWilliams, 2024) and direct-numerical simulations;
2. The BOD23 frontal width is based on near-surface frontal width measured in LES of turbulence-arrested frontogenesis, while SBI depends on the width of the front over the whole mixed layer; this suggests that the value of $C_r(t,y,x)$ found optimal in BOD23 may be larger than the diagnosed or tuned values found here.

The implications are that BOD23 is sensitive to the choice of OSBL turbulence parameterization, due to the suggested relationship (3) and the fact that many metrics examined here (MLD, ventilation and AMOC) emerge from a coupling between OSBL mixing schemes and restratification schemes. Here, the MLE schemes are varied between BFF11 or BOD23 for each model, but other restratification mechanisms such as solar and upfront Ekman buoyancy flux are also present. Even if they are formulated identically, these mechanisms are expected to be sensitive to different vertical resolutions (Aguiar et al., 2025; Jia et al., 2021; Li et al., 2019; Ménesguen et al., 2025; Stewart & Hogg, 2019), water-type parameterizations (Paulson & Simpson, 1977), and OSBL mixing schemes (Li et al., 2021), which differ across the models. The tuning of C_r in each model attempts to compensate for these confounding effects, but our results indicate that this tuning is insufficient to make the BFF11 versus BOD23 results fully consistent in the face of diverse model-specific choices. BLOM uses KPP, CESM adopts a new KPP scheme which includes the effects of waves, and GFDL has ePBL. Namely, they all differ and were tuned with different goals in mind: GFDL was aiming for global heat content while BLOM and CESM tried to match the MLE stream functions $\left(\Psi^{\mathrm{BOD23}} \sim \Psi^{\mathrm{BFF11}}\right)$.

On the other hand, the shallower MLDs by BFF11 at lower latitudes are likely due to L_{ML} becoming ill defined. The reliance on L_{ML} in the BFF11 scheme was based on limited observational evidence (Hosegood et al., 2006) and heuristic arguments; a recent analysis (Whalen & Drushka, 2025) supports this case under some circumstances. However, these arguments and observations do not apply in the tropics, and the form of the BFF11 scheme as $f \to 0$ was theoretical rather than observationally justified. Furthermore, the $M^2\left(=|\nabla_{\mathrm{h}}\overline{b}^{z}|^2\right)$-based versions of BFF11 prescribe limits on L_f from both above and below (Fox-Kemper et al., 2011, their Equation 13), which unfortunately leads to a sensitivity to the setting of these artificial caps. This sensitivity is one motivating reason for BOD23 and the present study where we intercompare the combination of different schemes. Observations establish the net result of frontal arrest, mixing, and restratification, not the individual processes that lead to them, which are all parameterized in global ocean simulations. Thus, there are many feedbacks that need to be correctly sized for the frontal width and deformation radius to numerically converge as they do in observations.

The sensitivity of large-scale stratification to MLE parametrizations is consistent with Smith et al. (2025). Mesoscale dynamics in Smith et al. and in CESM and BLOM are parametrized by GM and isopycnic tracer diffusion. Non-eddying numerical simulations with GM turned on are notorious for being sensitive to the surface boundary conditions in computing the GM eddy-induced stream function (Gnanadesikan, Griffies, & Samuels, 2007; Danabasoglu et al., 2008; Ferrari et al., 2008, 2010; Uchida, 2019, his Appendix D). The MLE parametrizations in effect modify the boundary conditions for GM and indirectly affect the resulting interior stratification. This change in stratification in turn, likely modulates the ventilation of the global ocean via isopycnic tracer diffusion; the two have been shown to be interlinked (Gnanadesikan et al., 2015; Gnanadesikan, Russell, & Zeng, 2007; Jones & Abernathey, 2019). It would be interesting to test whether the mesoscale parametrization proposed by Greatbatch and Lamb (1990) would present similar levels of sensitivity to boundary conditions (cf., Loose et al., 2023). At the resolution of $1/4°$, mesoscale eddies are partially admitted in the GFDL runs but MLEs are not. The difference between the no-MLE run and BOD23-BFF11 twin runs highlights the sensitivity of MLD and ocean heat uptake to the interaction between MLE and OSBL schemes (Figures 1a, 3a, and 3b and Figure S1 in Supporting Information S1).

Nonetheless, overall, both BFF11 and BOD23 and Bodner et al. (2025) have very similar magnitudes of restratification when compared to using no submesoscale parameterization at all. Despite the differences in Figures 3c–3h, the spatial patterns between mixed-layer restratification in GFDL BFF11 and BOD23 in reference to the no-MLE run are very similar (Figure S1 in Supporting Information S1). This is also evident in the globally averaged temperature where the GFDL BFF11-BOD23 twin runs are cooler by $\mathcal{O}(1\,°\mathrm{C})$ than their no-MLE counterpart (blue and gray curves in Figure 1a). While this may seem small, given that the surface warming discussed in Intergovernmental Panel on Climate Change reports is on the order of 1.5 °C (Masson-Delmotte et al., 2018), the impact of MLE parametrizations on ocean heat uptake is non-negligible. Based on our results, we also recommend the relation $C_r < C_e$. Conversely, the tuned values of C_r (0.003–0.038) imply that the coefficient C_L be adjusted to 1.5–4, suggesting that symmetric instability may dominate as the frontal-arrest mechanism (Bachman et al., 2017; Dong et al., 2024). To summarize, our results highlight that it is better to use a submesoscale restratification scheme of some sort (cf. Zhang et al., 2025; Feng et al., 2025), but the large-scale, low-frequency ocean behavior is sensitive to the differences between BFF11 and BOD23 and their interaction with OSBL schemes. We have documented this via climate relevant metrics centered around global ocean heat and carbon uptake. In our opinion, the BOD23 parameterization better encapsulates the present understanding of boundary-layer processes than BFF11.

Conflict of Interest

The authors declare no conflicts of interest relevant to this study.

Data Availability Statement

The source code for GFDL MOM6, CESM MOM6 and BLOM can be accessed via Adcroft et al. (2019, https://github.com/NOAA-GFDL/MOM6.git), Marques et al. (2023, https://github.com/ESCOMP/MOM_interface/wiki/Detailed-Instructions) and Seland et al. (2020, https://github.com/NorESMhub/BLOM) respectively. Atlantic Meridional Overturning Circulation diagnostics were executed using the `xoverturning` Python package (Dussin & Krasting, 2021). The eNATL60 and HYCOM50 model outputs used in this paper are publicly available

on the Open Storage Network (OSN; https://www.openstoragenetwork.org/), a cloud storage platform operated by the NSF. Jupyter notebooks used for analyses are available via Github (Bodner & Uchida, 2025, https://doi.org/10.5281/zenodo.17872555). Other example Jupyter notebooks and Yaml file used to access the eNATL60 and HYCOM50 data can also be found on Github (Stern et al., 2022, https://github.com/pangeo-data/swot_adac_ogcms). Postprocessing of the eNATL60 and HYCOM50 outputs were done using the `xgcm` Python package (Abernathey et al., 2021). Thermodynamic diagnostics of eNATL60 and HYCOM50 were executed using the TEOS-10 `gsw` and `fastjmd95` Python packages respectively (Abernathey & Busecke, 2020; Firing et al., 2021; McDougall & Barker, 2011). Wavenumber spectra were computed using the `xrft` Python package (Uchida et al., 2023). We thank the developers of the `gcm-filters` Python package (Loose et al., 2022).

Acknowledgments
We acknowledge the editor Angelicque White, associate editor and two anonymous reviewers for their constructive comments. We thank the French MultiscalE Ocean Modeling (MEOM) and Center for Ocean-Atmospheric Prediction Studies modeling groups for making their simulation outputs publicly available via OSN. T. Uchida was supported through the National Science Foundation (NSF) Grants OCE-2123632 and OCE-1941963 during his time in the U.S. and the Moscow Institute of Physics and Technology Development Program (Priority-2030) upon moving to Russia. A. Bodner was supported by a Grant from the Simons Foundation: award number 855143, Bodner. M. Ilicak and M. Bentsen were supported by the Research Council of Norway project INES2 (350390) and computing and storage resources for BLOM simulations provided by Norwegian infrastructure for computational science (through projects NN9560K and NS9560K). M. Ilicak was also partially supported by the Research Fund of the Istanbul Technical University ITU-TGA-2020-42517 and ITU-MGA-2025-46517 projects. GM is partially supported by the NSF Grant 1912420. This material is based upon work supported by the National Center for Atmospheric Research, which is a major facility sponsored by the NSF under cooperative agreement no. 1852977. Computing resources (https://doi.org/10.5065/qx9a-pg09) were provided by the Climate Simulation Laboratory at NCAR's Computational and Information Systems Laboratory, sponsored by the NSF and other agencies. We thank John P. Krasting for helpful comments on a draft of this manuscript.

References

Abdulah, S., Baker, A. H., Bosilca, G., Cao, Q., Castruccio, S., Genton, M. G., et al. (2024). Boosting Earth system model outputs and saving petabytes in their storage using exascale climate emulators. In *Proceedings of the international conference for high performance computing, networking, storage, and analysis*. IEEE Press. https://doi.org/10.1109/SC41406.2024.00008

Abernathey, R. P., & Busecke, J. J. M. (2020). fastjmd95: Numba implementation of Jackett & McDougall (1995) ocean equation of state [Software]. *Zenodo*. https://doi.org/10.5281/zenodo.4498376

Abernathey, R. P., Busecke, J. J. M., Smith, T., Banihirwe, A., Fernandes, F., & Bourbeau, J. (2021). Xgcm: General Circulation Model Post-processing with xarray [Software]. *Zenodo*. https://doi.org/10.5281/zenodo.3634752

Adcroft, A., Anderson, W., Balaji, V., Blanton, C., Bushuk, M., Dufour, C. O., et al. (2019). The GFDL global ocean and sea ice model OM4.0: Model description and simulation features. *Journal of Advances in Modeling Earth Systems*, *11*(10), 3167–3211. https://doi.org/10.1029/2019MS001726

Aguiar, W., Morrison, A. K., Huneke, W. G., Hutchinson, D. K., Spence, P., Hogg, A. M., et al. (2025). Antarctic dense water formation sensitivity to ocean surface cell thickness. *Journal of Advances in Modeling Earth Systems*, *17*(7), e2024MS004913. https://doi.org/10.1029/2024MS004913

Ajayi, A., Le Sommer, J., Chassignet, E. P., Molines, J.-M., Xu, X., Albert, A., & Cosme, E. (2020). Spatial and temporal variability of the north atlantic eddy field from two kilometric-resolution ocean models. *Journal of Geophysical Research: Oceans*, *125*(5), e2019JC015827. https://doi.org/10.1029/2019JC015827

Ajayi, A., Le Sommer, J., Chassignet, E. P., Molines, J.-M., Xu, X., Albert, A., & Dewar, W. K. (2021). Diagnosing cross-scale kinetic energy exchanges from two submesoscale permitting ocean models. *Journal of Advances in Modeling Earth Systems*, *13*(6), e2019MS001923. https://doi.org/10.1029/2019MS001923

Bachman, S. D., Fox-Kemper, B., Taylor, J. R., & Thomas, L. N. (2017). Parameterization of frontal symmetric instabilities. I: Theory for resolved fronts. *Ocean Modelling*, *109*, 72–95. https://doi.org/10.1016/j.ocemod.2016.12.003

Bai, Y., Thompson, A. F., Bôas, A. B. V., Klein, P., Torres, H. S., & Menemenlis, D. (2023). Sub-mesoscale wind-front interactions: The combined impact of thermal and current feedback. *Geophysical Research Letters*, *50*(18), e2023GL104807. https://doi.org/10.1029/2023gl104807

Boccaletti, G., Ferrari, R., & Fox-Kemper, B. (2007). Mixed layer instabilities and restratification. *Journal of Physical Oceanography*, *37*(9), 2228–2250. https://doi.org/10.1175/jpo3101.1

Bodner, A., Balwada, D., & Zanna, L. (2025). A data-driven approach for parameterizing ocean submesoscale buoyancy fluxes. *Journal of Advances in Modeling Earth Systems*, *17*(11), e2025MS004991. https://doi.org/10.1029/2025MS004991

Bodner, A., & Uchida, T. (2025). Submeso_param_mle: Jupyter notebook repository for diagnosing MLE parametrizations [Software]. *Zenodo*. https://doi.org/10.5281/zenodo.17872555

Bodner, A. S., Fox-Kemper, B., Johnson, L., Roekel, L. P. V., McWilliams, J. C., Sullivan, P. P., et al. (2023). Modifying the mixed layer eddy parameterization to include frontogenesis arrest by boundary layer turbulence. *Journal of Physical Oceanography*, *53*(1), 323–339. https://doi.org/10.1175/jpo-d-21-0297.1

Boyd, P. W., Claustre, H., Levy, M., Siegel, D. A., & Weber, T. (2019). Multi-faceted particle pumps drive carbon sequestration in the ocean. *Nature*, *568*(7752), 327–335. https://doi.org/10.1038/s41586-019-1098-2

Boyer, T. P., Garcia, H. E., Locarnini, R. A., Zweng, M. M., Mishonov, A. V., Reagan, J. R., et al. (2018). *World Ocean Atlas 2018*. NOAA National Centers for Environmental Information. Retrieved from https://www.ncei.noaa.gov/archive/accession/NCEI-WOA18

Brodeau, L., Albert, A., & Le Sommer, J. (2020). NEMO-eNATL60 description and assessment repository. https://doi.org/10.5281/zenodo.4032732

Buckingham, C. E., Lucas, N. S., Belcher, S. E., Rippeth, T. P., Grant, A. L., Le Sommer, J., et al. (2019). The contribution of surface and submesoscale processes to turbulence in the open ocean surface boundary layer. *Journal of Advances in Modeling Earth Systems*, *11*(12), 4066–4094. https://doi.org/10.1029/2019MS001801

Busecke, J. J., Balwada, D., Martin, P. E., Nicholas, T. E., Johnson, Z. C., Nalluri, P., et al. (2025). The impact of sub-grid heterogeneity on air-sea turbulent heat flux in coupled climate models. *Geophysical Research Letters*, *52*(13), e2025GL114951. https://doi.org/10.1029/2025GL114951

Busecke, J. J., Resplandy, L., Ditkovsky, S. J., & John, J. G. (2022). Diverging fates of the Pacific Ocean oxygen minimum zone and its core in a warming world. *AGU Advances*, *3*(6), e2021AV000470. https://doi.org/10.1029/2021AV000470

Caesar, L., Rahmstorf, S., Robinson, A., Feulner, G., & Saba, V. (2018). Observed fingerprint of a weakening Atlantic Ocean overturning circulation. *Nature*, *556*(7700), 191–196. https://doi.org/10.1038/s41586-018-0006-5

Calvert, D., Nurser, G., Bell, M. J., & Fox-Kemper, B. (2020). The impact of a parameterisation of submesoscale mixed layer eddies on mixed layer depths in the NEMO ocean model. *Ocean Modelling*, *154*, 101678. https://doi.org/10.1016/j.ocemod.2020.101678

Chassignet, E. P., & Xu, X. (2017). Impact of horizontal resolution (1/12° to 1/50°) on gulf stream separation, penetration, and variability. *Journal of Physical Oceanography*, *47*(8), 1999–2021. https://doi.org/10.1175/jpo-d-17-0031.1

Chassignet, E. P., Yeager, S. G., Fox-Kemper, B., Bozec, A., Castruccio, F., & Danabasoglu, G. (2020). *Impact of horizontal resolution on global ocean-sea-ice model simulations based on the experimental protocols of the Ocean Model Intercomparison Project phase 2 (OMIP-2)* (pp. 1–58). Geoscientific Model Development. https://doi.org/10.5194/gmd-13-4595-2020

Conejero, C., Renault, L., Desbiolles, F., McWilliams, J., & Giordani, H. (2024). Near-surface atmospheric response to meso- and submesoscale current and thermal feedbacks. *Journal of Physical Oceanography*, *54*(3), 823–848. https://doi.org/10.1175/JPO-D-23-0211.1

Danabasoglu, G., Bates, S. C., Briegleb, B. P., Jayne, S. R., Jochum, M., Large, W. G., et al. (2012). The CCSM4 ocean component. *Journal of Climate*, *25*(5), 1361–1389. https://doi.org/10.1175/JCLI-D-11-00091.1

Danabasoglu, G., Ferrari, R., & McWilliams, J. C. (2008). Sensitivity of an ocean general circulation model to a parameterization of near-surface eddy fluxes. *Journal of Climate*, *21*(6), 1192–1208. https://doi.org/10.1175/2007JCLI1508.1

Danabasoglu, G., Yeager, S. G., Bailey, D., Behrens, E., Bentsen, M., Bi, D., et al. (2014). North Atlantic simulations in coordinated ocean-ice reference experiments phase II (CORE-II). Part I: Mean states. *Ocean Modelling*, *73*, 76–107. https://doi.org/10.1016/j.ocemod.2013.10.005

de Boyer Montégut, C., Madec, G., Fischer, A. S., Lazar, A., & Iudicone, D. (2004). Mixed layer depth over the global ocean: An examination of profile data and a profile-based climatology. *Journal of Geophysical Research*, *109*(C12). https://doi.org/10.1029/2004JC002378

De Marez, C., Ruiz-Angulo, A., & Le Corre, M. (2024). Structure of the bottom boundary current south of Iceland and spreading of deep waters by submesoscale processes. *Geophysical Research Letters*, *51*(5), e2023GL107508. https://doi.org/10.1029/2023GL107508

Deremble, B., & Dewar, W. K. (2013). Volume and potential vorticity budgets of eighteen degree water. *Journal of Physical Oceanography*, *43*(11), 2309–2321. https://doi.org/10.1175/JPO-D-13-052.1

Dewar, W. K. (1986). On the potential vorticity structure of weakly ventilated isopycnals: A theory of subtropical mode water maintenance. *Journal of Physical Oceanography*, *16*(7), 1204–1216. https://doi.org/10.1175/1520-0485(1986)016⟨1204:OTPVSO⟩2.0.CO;2

Dong, J., Fox-Kemper, B., Wenegrat, J., Bodner, A. S., Yu, X., Belcher, S., & Dong, C. (2024). Submesoscales are a significant turbulence source in global ocean surface boundary layer. *Nature Communications*, *15*(9566), 9566. https://doi.org/10.1038/s41467-024-53959-y

Dong, J., Fox-Kemper, B., Zhang, H., & Dong, C. (2020). The scale of submesoscale baroclinic instability globally. *Journal of Physical Oceanography*, *50*(9), 2649–2667. https://doi.org/10.1175/jpo-d-20-0043.1

Dong, J., Fox-Kemper, B., Zhang, H., & Dong, C. (2021). The scale and activity of symmetric instability estimated from a global submesoscale-permitting ocean model. *Journal of Physical Oceanography*, *51*(5), 1655–1670. https://doi.org/10.1175/jpo-d-20-0159.1

Dussin, R., & Krasting, J. (2021). Xoverturning: MOM6 ocean overturning in xarray [Software]. https://github.com/raphaeldussin/xoverturning

Eyring, V., Bony, S., Meehl, G. A., Senior, C. A., Stevens, B., Stouffer, R. J., & Taylor, K. E. (2016). Overview of the coupled model intercomparison project Phase 6 (CMIP6) experimental design and organization. *Geoscientific Model Development*, *9*(5), 1937–1958. https://doi.org/10.5194/gmd-9-1937-2016

Feng, Z., Zhang, Z., Zhang, J., Zhang, W., Yuan, M., Jing, Z., et al. (2025). Implementation and evaluation of a new parameterization of submesoscale vertical flux in a mesoscale-resolving model in the North Pacific. *Ocean Modelling*, *199*, 102655. https://doi.org/10.1016/j.ocemod.2025.102655

Ferrari, R., Griffies, S. M., Nurser, A. G., & Vallis, G. K. (2010). A boundary-value problem for the parameterized mesoscale eddy transport. *Ocean Modelling*, *32*(3–4), 143–156. https://doi.org/10.1016/j.ocemod.2010.01.004

Ferrari, R., McWilliams, J. C., Canuto, V. M., & Dubovikov, M. (2008). Parameterization of eddy fluxes near oceanic boundaries. *Journal of Climate*, *21*(12), 2770–2789. https://doi.org/10.1175/2007JCLI1510.1

Firing, E., Fernandes, F., Barna, A., & Abernathey, R. P. (2021). TEOS-10/GSW-Python: V3.4.1.post0 [Software]. *Zenodo*. https://doi.org/10.5281/zenodo.5214122

Forget, G., Maze, G., Buckley, M., & Marshall, J. (2011). Estimated seasonal cycle of North Atlantic Eighteen Degree water volume. *Journal of Physical Oceanography*, *41*(2), 269–286. https://doi.org/10.1175/2010jpo4257.1

Fox-Kemper, B., Bachman, S., Pearson, B., & Reckinger, S. (2014). Principles and advances in subgrid modeling for eddy-rich simulations. *CLIVAR Exchanges*, *19*(2), 42–46.

Fox-Kemper, B., Danabasoglu, G., Ferrari, R., Griffies, S., Hallberg, R., Holland, M., et al. (2011). Parameterization of mixed layer eddies. III: Implementation and impact in global ocean climate simulations. *Ocean Modelling*, *39*(1–2), 61–78. https://doi.org/10.1016/j.ocemod.2010.09.002

Fox-Kemper, B., Ferrari, R., & Hallberg, R. (2008). Parameterization of mixed layer eddies. Part I: Theory and diagnosis. *Journal of Physical Oceanography*, *38*(6), 1145–1165. https://doi.org/10.1175/2007JPO3792.1

Fox-Kemper, B., Hewitt, H. T., Xiao, C., Adalgeirsdottir, G., Drijfhout, S. S., Edwards, T. L., et al. (2021). *Climate change 2021: The physical science basis. Contribution of working Group I to the sixth assessment report of the intergovernmental panel on climate change*. In V. Masson-Delmotte et al. (Eds.), (pp. 1211–1362). : Cambridge University Press. https://doi.org/10.1017/9781009157896.011

Gent, P. R., & McWilliams, J. C. (1990). Isopycnal mixing in ocean circulation models. *Journal of Physical Oceanography*, *20*(1), 150–155. https://doi.org/10.1175/1520-0485(1990)020⟨0150:IMIOCM⟩2.0.CO;2

Gnanadesikan, A., Griffies, S. M., & Samuels, B. L. (2007). Effects in a climate model of slope tapering in neutral physics schemes. *Ocean Modelling*, *16*(1–2), 1–16. https://doi.org/10.1016/j.ocemod.2006.06.004

Gnanadesikan, A., Pradal, M.-A., & Abernathey, R. P. (2015). Isopycnal mixing by mesoscale eddies significantly impacts oceanic anthropogenic carbon uptake. *Geophysical Research Letters*, *42*(11), 4249–4255. https://doi.org/10.1002/2015GL064100

Gnanadesikan, A., Russell, J., & Zeng, F. (2007). How does ocean ventilation change under global warming? *Ocean Science*, *3*(1), 43–53. https://doi.org/10.5194/os-3-43-2007

Govett, M., Bah, B., Bauer, P., Berod, D., Bouchet, V., Corti, S., et al. (2024). Exascale computing and data handling: Challenges and opportunities for weather and climate prediction. *Bulletin of the American Meteorological Society*, *105*(12), E2385–E2404. https://doi.org/10.1175/BAMS-D-23-0220.1

Greatbatch, R. J., & Lamb, K. G. (1990). On parameterizing vertical mixing of momentum in non-eddy resolving ocean models. *Journal of Physical Oceanography*, *20*(10), 1634–1637. https://doi.org/10.1175/1520-0485(1990)020⟨1634:OPVMOM⟩2.0.CO;2

Griffies, S. M. (2018). *Fundamentals of ocean climate models*. Princeton university press.

Griffies, S. M., Adcroft, A., Beadling, R. L., Bushuk, M., Chang, C.-Y., Drake, H. F., et al. (2025a). The GFDL-CM4X climate model hierarchy, Part II: Case studies. *Journal of Advances in Modeling Earth Systems*, *17*(10), e2024MS004862. https://doi.org/10.1029/2024MS004862

Griffies, S. M., Adcroft, A., Beadling, R. L., Bushuk, M., Chang, C.-Y., Drake, H. F., et al. (2025b). The GFDL-CM4X climate model hierarchy, Part I: Model description and thermal properties. *Journal of Advances in Modeling Earth Systems*, *17*(10), e2024MS004861. https://doi.org/10.1029/2024MS004861

Griffies, S. M., Danabasoglu, G., Durack, P. J., Adcroft, A. J., Balaji, V., Böning, C. W., et al. (2016). OMIP contribution to CMIP6: Experimental and diagnostic protocol for the physical component of the Ocean Model Intercomparison Project. *Geoscientific Model Development*, *3231*(9), 3231–3296. https://doi.org/10.5194/gmd-9-3231-2016

Griffies, S. M., & Greatbatch, R. J. (2012). Physical processes that impact the evolution of global mean sea level in ocean climate models. *Ocean Modelling*, *51*, 37–72. https://doi.org/10.1016/j.ocemod.2012.04.003

Griffies, S. M., Levy, M., Adcroft, A. J., Danabasoglu, G., Hallberg, R. W., Jacobsen, D., et al. (2015). Theory and numerics of the community ocean vertical mixing (CVMix) Project. (Technical Report). Retrieved from https://github.com/CVMix/CVMix-description/blob/master/cvmix.pdf

Grooms, I., Loose, N., Abernathey, R. P., Steinberg, J. M., Bachman, S. D., Marques, G., et al. (2021). Diffusion-based smoothers for spatial filtering of gridded geophysical data. *Journal of Advances in Modeling Earth Systems*, *13*(9), e2021MS002552. https://doi.org/10.1029/2021MS002552

Häfner, D., Nuterman, R., & Jochum, M. (2021). Fast, cheap, and turbulent-global ocean modeling with GPU acceleration in Python. *Journal of Advances in Modeling Earth Systems*, *13*(12), e2021MS002717. https://doi.org/10.1029/2021MS002717

Hewitt, H., Fox-Kemper, B., Pearson, B., Roberts, M., & Klocke, D. (2022). The small scales of the ocean may hold the key to surprises. *Nature Climate Change*, *12*(6), 496–499. https://doi.org/10.1038/s41558-022-01386-6

Hosegood, P., Gregg, M. C., & Alford, M. H. (2006). Sub-mesoscale lateral density structure in the oceanic surface mixed layer. *Geophysical Research Letters*, *33*(22). https://doi.org/10.1029/2006GL026797

Jackson, L., Hallberg, R., & Legg, S. (2008). A parameterization of shear-driven turbulence for ocean climate models. *Journal of Physical Oceanography*, *38*(5), 1033–1053. https://doi.org/10.1175/2007JPO3779.1

Jamet, Q., Berger, A., Deremble, B., & Penduff, T. (2024). Thermodynamical effects of ocean current feedback in a quasi-geostrophic coupled model. *Journal of Physical Oceanography*, *54*(8), 1691–1704. https://doi.org/10.1175/JPO-D-23-0159.1

Jayne, S. R. (2009). The impact of abyssal mixing parameterizations in an ocean general circulation model. *Journal of Physical Oceanography*, *39*(7), 1756–1775. https://doi.org/10.1175/2009JPO4085.1

Jia, Y., Richards, K. J., & Annamalai, H. (2021). The impact of vertical resolution in reducing biases in sea surface temperature in a tropical Pacific Ocean model. *Ocean Modelling*, *157*, 101722. https://doi.org/10.1016/j.ocemod.2020.101722

Johnson, L., & Fox-Kemper, B. (2024). Modification of boundary layer turbulence by submesoscale flows. *Flowline*, *4*, E20. https://doi.org/10.1017/flo.2024.17

Johnson, L., Lee, C. M., & D'Asaro, E. A. (2016). Global estimates of lateral springtime restratification. *Journal of Physical Oceanography*, *46*(5), 1555–1573. https://doi.org/10.1175/jpo-d-15-0163.1

Johnson, L., Lee, C. M., D'Asaro, E. A., Thomas, L., & Shcherbina, A. (2020). Restratification at a California current upwelling front, part 1: Observations. *Journal of Physical Oceanography*, *50*(5), 1455–1472. https://doi.org/10.1175/JPO-D-19-0203.1

Jones, S. C., & Abernathey, R. P. (2019). Isopycnal mixing controls deep ocean ventilation. *Geophysical Research Letters*, *46*(22), 13144–13151. https://doi.org/10.1029/2019gl085208

Large, W. G., McWilliams, J. C., & Doney, S. C. (1994). Oceanic vertical mixing: A review and a model with a nonlocal boundary layer parameterization. *Reviews of Geophysics*, *32*(4), 363–403. https://doi.org/10.1029/94rg01872

Large, W. G., Patton, E. G., & Sullivan, P. P. (2021). The diurnal cycle of entrainment and detrainment in LES of the Southern Ocean driven by observed surface fluxes and waves. *Journal of Physical Oceanography*, *51*(10), 3253–3278. https://doi.org/10.1175/JPO-D-20-0308.1

Levitus, S., Boyer, T. P., Garcia, H. E., Locarnini, R. A., Zweng, M. M., Mishonov, A. V., et al. (2014). *World Ocean Atlas 2013 (NCEI Accession 0114815)*. NOAA National Centers for Environmental Information. https://doi.org/10.7289/v5f769gt

Lévy, M., Bopp, L., Karleskind, P., Resplandy, L., Éthé, C., & Pinsard, F. (2013). Physical pathways for carbon transfers between the surface mixed layer and the ocean interior. *Global Biogeochemical Cycles*, *27*(4), 1001–1012. https://doi.org/10.1002/gbc.20092

Li, G., Wang, D., Dong, C., Pan, J., Shu, Y., & Zhang, Z. (2024). Frontogenesis and frontolysis of a cold filament driven by the cross-filament wind and wave fields simulated by a large eddy simulation. *Advances in Atmospheric Sciences*, *41*(3), 509–528. https://doi.org/10.1007/s00376-023-3037-2

Li, Q., Bruggeman, J., Burchard, H., Klingbeil, K., Umlauf, L., & Bolding, K. (2021). Integrating CVMix into GOTM (v6.0): A consistent framework for testing, comparing, and applying ocean mixing schemes. *Geoscientific Model Development*, *2021*(7), 1–30. https://doi.org/10.5194/gmd-14-4261-2021

Li, Q., Reichl, B. G., Fox-Kemper, B., Adcroft, A. J., Belcher, S. E., Danabasoglu, G., et al. (2019). Comparing ocean surface boundary vertical mixing schemes including langmuir turbulence. *Journal of Advances in Modeling Earth Systems*, *11*(11), 3545–3592. https://doi.org/10.1029/2019MS001810

Loose, N., Abernathey, R. P., Grooms, I., Busecke, J. J. M., Guillaumin, A. P., Yankovsky, E., et al. (2022). GCM-filters: A python package for diffusion-based spatial filtering of gridded data. *Journal of Open Source Software*, *7*(70), 3947. https://doi.org/10.21105/joss.03947

Loose, N., Marques, G. M., Adcroft, A., Bachman, S. D., Griffies, S. M., Grooms, I., et al. (2023). Comparing two parameterizations for the restratification effect of mesoscale eddies in an isopycnal ocean model. *Journal of Advances in Modeling Earth Systems*, *15*(12), e2022MS003518. https://doi.org/10.1029/2022MS003518

Mahadevan, A., D'asaro, E., Lee, C., & Perry, M. J. (2012). Eddy-driven stratification initiates North Atlantic spring phytoplankton blooms. *Science*, *337*(6090), 54–58. https://doi.org/10.1126/science.1218740

Marques, G. M., Shao, A. E., Bachman, S. D., Danabasoglu, G., & Bryan, F. O. (2023). Representing eddy diffusion in the surface boundary layer of ocean models with general vertical coordinates. *Journal of Advances in Modeling Earth Systems*, *15*(6), e2023MS003751. https://doi.org/10.1029/2023MS003751

Masson-Delmotte, V., Zhai, P., Pirani, A., Connors, S. L., Péan, C., & Berger, S. (2021). Climate Change 2021: The Physical Science Basis. Contribution of working group I to the sixth assessment report of the intergovernmental Panel on. *Climate Change*, *2*(1), 2391. https://doi.org/10.1017/9781009157896

Masson-Delmotte, V., Zhai, P., Pörtner, H.-O., Roberts, D., Skea, J., & Shukla, P. R. (2018). Global warming of 1.5 C. *Intergovernmental Panel on Climate Change (IPCC)*, *1*(5), 43–50. Retrieved from https://www.ipcc.ch/sr15/

Maze, G., & Marshall, J. (2011). Diagnosing the observed seasonal cycle of Atlantic subtropical mode water using potential vorticity and its attendant theorems. *Journal of Physical Oceanography*, *41*(10), 1986–1999. https://doi.org/10.1175/2011jpo4576.1

McDougall, T. J., & Barker, P. M. (2011). *Getting started with TEOS-10 and the Gibbs seawater (GSW) oceanographic toolbox*. SCOR/IAPSO WG127. Retrieved from https://www.teos-10.org/pubs/Getting_Started.pdf

Ménesguen, C., Ducousso, N., Vic, C., & Le Gentil, S. (2025). Exploring baroclinic instability of the computational kind (BICK) in numerical simulations of the ocean. *Journal of Advances in Modeling Earth Systems*, *17*(4), e2024MS004600. https://doi.org/10.1029/2024MS004600

Moon, J.-Y., Streffing, J., Lee, S.-S., Semmler, T., Andrés-Martínez, M., Chen, J., et al. (2025). Earth's future climate and its variability simulated at 9 km global resolution. *Earth System Dynamics*, *16*(4), 1103–1134. https://doi.org/10.5194/esd-16-1103-2025

Naveira Garabato, A. C., MacGilchrist, G. A., Brown, P. J., Evans, D. G., Meijers, A. J., & Zika, J. D. (2017). High-latitude ocean ventilation and its role in Earth's climate transitions. *Philosophical Transactions of the Royal Society A: Mathematical, Physical and Engineering Sciences*, *375*(2102), 20160324. https://doi.org/10.1098/rsta.2016.0324

Nummelin, A., & Isachsen, P. E. (2024). Parameterizing mesoscale eddy buoyancy transport over sloping topography. *Journal of Advances in Modeling Earth Systems*, *16*(3), e2023MS003806. https://doi.org/10.1029/2023MS003806

Orr, J. C., Najjar, R. G., Aumont, O., Bopp, L., Bullister, J. L., Danabasoglu, G., et al. (2017). Biogeochemical protocols and diagnostics for the CMIP6 ocean model intercomparison project (OMIP). *Geoscientific Model Development*, *10*(6), 2169–2199. https://doi.org/10.5194/gmd-10-2169-2017

Panta, A., Huang, X., McCurdy, N., Ellsworth, D., Gooch, A. A., Scorzelli, G., et al. (2024). Web-based visualization and analytics of petascale data: Equity as a tide that lifts all boats. In *2024 ieee 14th symposium on large data analysis and visualization (ldav)* (pp. 1–11). https://doi.org/10.1109/LDAV64567.2024.00009

Paulson, C. A., & Simpson, J. J. (1977). Irradiance measurements in the upper ocean. *Journal of Physical Oceanography*, *7*(6), 952–956. https://doi.org/10.1175/1520-0485(1977)007⟨0952:IMITUO⟩2.0.CO;2

Redi, M. H. (1982). Oceanic isopycnal mixing by coordinate rotation. *Journal of Physical Oceanography*, *12*(10), 1154–1158. https://doi.org/10.1175/1520-0485(1982)012⟨1154:OIMBCR⟩2.0.CO;2

Reichl, B. G., & Hallberg, R. (2018). A simplified energetics based planetary boundary layer (ePBL) approach for ocean climate simulations. *Ocean Modelling*, *132*, 112–129. https://doi.org/10.1016/j.ocemod.2018.10.004

Reichl, B. G., Wittenberg, A. T., Griffies, S. M., & Adcroft, A. (2024). Improving equatorial upper ocean vertical mixing in the NOAA/GFDL OM4 model. *Earth and Space Science*, *11*(10), e2023EA003485. https://doi.org/10.1029/2023EA003485

Seland, Ø., Bentsen, M., Olivié, D., Toniazzo, T., Gjermundsen, A., Graff, L. S., et al. (2020). Overview of the Norwegian Earth System Model (NorESM2) and key climate response of CMIP6 DECK, historical, and scenario simulations. *Geoscientific Model Development*, *13*(12), 6165–6200. https://doi.org/10.5194/gmd-13-6165-2020

Shao, A. E., Adcroft, A., Hallberg, R., & Griffies, S. M. (2020). A general-coordinate, non-local neutral diffusion operator. *Journal of Advances in Modeling Earth Systems*, *12*(12), e2019MS001992. https://doi.org/10.1029/2019MS001992

Silvestri, S., Wagner, G. L., Constantinou, N. C., Hill, C. N., Campin, J.-M., Souza, A. N., et al. (2025). A GPU-Based ocean dynamical core for routine mesoscale-resolving climate simulations. *Journal of Advances in Modeling Earth Systems*, *17*(4), e2024MS004465. https://doi.org/10.1029/2024MS004465

Silvestri, S., Wagner, G. L., Hill, C. N., Ardakani, M. R., Blaschke, J., & Campin, J.-M. (2023). *Oceananigans.jl: A model that achieves breakthrough resolution, memory and energy efficiency in global ocean simulations*. arXiv. https://doi.org/10.48550/arXiv.2309.06662

Simmons, H. L., Jayne, S. R., Laurent, L. C. S., & Weaver, A. J. (2004). Tidally driven mixing in a numerical model of the ocean general circulation. *Ocean Modelling*, *6*(3–4), 245–263. https://doi.org/10.1016/S1463-5003(03)00011-8

Smith, K., Barthel, A. M., Conlon, L. M., Van Roekel, L. P., Bartoletti, A., Golez, J.-C., et al. (2025). The DOE E3SM version 2.1: Overview and assessment of the impacts of parameterized ocean submesoscales. *Geoscientific Model Development*, *2025*(5), 1–38. https://doi.org/10.5194/gmd-18-1613-2025

Steele, M., Morley, R., & Ermold, W. (2001). PHC: A global ocean hydrography with a high-quality Arctic Ocean. *Journal of Climate*, *14*(9), 2079–2087. https://doi.org/10.1175/1520-0442(2001)014⟨2079:PAGOHW⟩2.0.CO;2

Stern, C. I., Uchida, T., & Abernathey, R. P. (2022). Swot_adac_ogcms: Documentation and notebooks for the SWT Adopt-a-Crossover Model Intercomparison [Software]. https://doi.org/10.5281/zenodo.6762535

Stewart, K., & Hogg, A. M. (2019). Southern Ocean heat and momentum uptake are sensitive to the vertical resolution at the ocean surface. *Ocean Modelling*, *143*, 101456. https://doi.org/10.1016/j.ocemod.2019.101456

Stone, P. H. (1966). On non-geostrophic baroclinic stability. *Journal of the Atmospheric Sciences*, *23*(4), 390–400. https://doi.org/10.1175/1520-0469(1966)023⟨0390:ONGBS⟩2.0.CO;2

Storkey, D., Mathiot, P., Bell, M. J., Copsey, D., Guiavarc'h, C., Hewitt, H. T., et al. (2024). Resolution dependence of interlinked Southern Ocean biases in global coupled HadGEM3 models. *EGUsphere*, *2024*, 1–29. https://doi.org/10.5194/egusphere-2024-1414

Sullivan, P. P., & McWilliams, J. C. (2024). Oceanic frontal turbulence. *Journal of Physical Oceanography*, *54*(2), 333–358. https://doi.org/10.1175/JPO-D-23-0033.1

Sun, L., Uchida, T., Penduff, T., Dewar, W. K., Deremble, B., Poje, A. C., et al. (2025). On the dynamics of the subtropical mode water from an ensemble view. *Authorea Preprints*. https://doi.org/10.22541/essoar.174802928.80389595/v1

Sutherland, G., Reverdin, G., Marié, L., & Ward, B. (2014). Mixed and mixing layer depths in the ocean surface boundary layer under conditions of diurnal stratification. *Geophysical Research Letters*, *41*(23), 8469–8476. https://doi.org/10.1002/2014GL061939

Tagklis, F., Bracco, A., Ito, T., & Castelao, R. (2020). Submesoscale modulation of deep water formation in the Labrador sea. *Scientific Reports*, *10*(1), 1–13. https://doi.org/10.1038/s41598-020-74345-w

Treguier, A. M., de Boyer Montégut, C., Bozec, A., Chassignet, E. P., Fox-Kemper, B., McC. Hogg, A., et al. (2023). The mixed-layer depth in the ocean model intercomparison project (OMIP): Impact of resolving mesoscale eddies. *Geoscientific Model Development*, *16*(13), 3849–3872. https://doi.org/10.5194/gmd-16-3849-2023

Tsujino, H., Urakawa, S., Nakano, H., Small, R. J., Kim, W. M., Yeager, S. G., et al. (2018). JRA-55 based surface dataset for driving ocean–sea-ice models (JRA55-do). *Ocean Modelling*, *130*, 79–139. https://doi.org/10.1016/j.ocemod.2018.07.002

Uchida, T. (2019). *Seasonality in surface (sub)mesoscale turbulence and its impact on iron transport and primary production*. (Doctoral dissertation). Columbia University in the City of New York). https://doi.org/10.7916/d8-9s8r-m049

Uchida, T., Abernathey, R. P., & Smith, K. S. (2017). Seasonality of eddy kinetic energy in an eddy permitting global climate model. *Ocean Modelling*, *118*, 41–58. https://doi.org/10.1016/j.ocemod.2017.08.006

Uchida, T., Balwada, D., Abernathey, R. P., McKinley, G. A., Smith, K. S., & Lévy, M. (2019). The contribution of submesoscale over mesoscale eddy iron transport in the open Southern Ocean. *Journal of Advances in Modeling Earth Systems*, *11*(12), 3934–3958. https://doi.org/10.1029/2019MS001805

Uchida, T., Balwada, D., Abernathey, R. P., McKinley, G. A., Smith, K. S., & Lévy, M. (2020). Vertical eddy iron fluxes support primary production in the open Southern Ocean. *Nature Communications*, *11*(1), 1125. https://doi.org/10.1038/s41467-020-14955-0

Uchida, T., Le Sommer, J., Stern, C. I., Abernathey, R. P., Holdgraf, C., Albert, A., et al. (2022). Cloud-based framework for inter-comparing submesoscale permitting realistic ocean models. *Geoscientific Model Development*, *15*(14), 5829–5856. https://doi.org/10.5194/gmd-15-5829-2022

Uchida, T., Rokem, A., Squire, D., Nicholas, T., Abernathey, R. P., & Soler, S. (2023). Xrft: Fourier transforms for Xarray data [Software]. *Zenodo*. https://doi.org/10.5281/zenodo.1402635

Wei, J., Han, X., Yu, J., Jiang, J., Liu, H., & Lin, P. (2024). A performance-portable kilometer-scale global ocean model on ORISE and new sunway heterogeneous supercomputers. In *2024 SC24: International conference for high performance computing, networking, storage and analysis* (pp. 1–24). https://doi.org/10.1109/SC41406.2024.00009

Whalen, C., & Drushka, K. (2025). Global distribution and governing dynamics of submesoscale density fronts. *Journal of Physical Oceanography*, *55*(10), 1831–1845. https://doi.org/10.1175/JPO-D-24-0119.1

Xu, L., Liu, J., Ding, Y., Sasaki, H., Cao, H., Dong, J., & Xing, L. (2025). Submesoscale effects on formation of the North Pacific subtropical mode water. *Journal of Physical Oceanography*, *55*(5), 559–572. https://doi.org/10.1175/JPO-D-24-0125.1

Xu, X., Chassignet, E. P., Wallcraft, A. J., Arbic, B. K., Buijsman, M. C., & Solano, M. (2022). On the spatial variability of the mesoscale sea surface height wavenumber spectra in the Atlantic Ocean. *Journal of Geophysical Research: Oceans*, *127*(10), e2022JC018769. https://doi.org/10.1029/2022JC018769

Zhang, S., Xu, S., Fu, H., Wu, L., Liu, Z., Gao, Y., et al. (2023). Toward Earth system modeling with resolved clouds and ocean submesoscales on heterogeneous many-core HPCs. *National Science Review*, *10*(6), nwad069. https://doi.org/10.1093/nsr/nwad069

Zhang, Z., An, B., Zhang, Z., Guo, Y., Zhang, J., Feng, Z., & Yu, Y. (2025). Local effect of a submesoscale parameterization scheme and its remote influences on large-scale circulation in the Northwest Pacific. *Ocean Modelling*, *199*, 102650. https://doi.org/10.1016/j.ocemod.2025.102650